Subhasree Dutta

Thermal and hydrodynamic analysis of viscoplastic flow in a channel-cavity system with temperature-dependent properties

Abstract: We perform numerical simulations to investigate heat transfer and mixed convection characteristics of a viscoplastic fluid moving through a grooved channel. To accurately capture the fluid behavior, we use a nonhomogeneous model. The results demonstrate the formation of distinct yielded and unyielded zones affected by variations in *Re* and *Ca*. An increase in *Re* promotes enhanced recirculation and reduces the extent of unyielded zones, whereas a higher *Ca* restricts fluid movement in regions where shear rates are low. The thermal field exhibits strong stratification at higher *Ri*, where buoyancy-driven thermal plumes enhance mixing and heat transfer, in contrast to uniform temperature profiles at lower *Ri*. Heat transfer analysis based on Nu_{av} highlights enhanced heat transport for higher φ_b and smaller d_p, with the nonhomogeneous model capturing significant contributions from Brownian diffusion and thermophoresis. Optimal heat transfer is achieved at high *Re* and low *Ca*, conditions that promote convective mixing and reduce unyielded regions. This study emphasizes the importance of nonhomogeneous modeling for accurate predictions in complex flow systems, offering valuable insights for optimizing thermal management in grooved channel applications.

Keywords: Nanofluid, open channel, two-phase model, viscoplastic fluid, entropy generation

1 Introduction

Open channels and those with open-bottom cavities have attracted considerable interest due to their versatility in engineering, with applications spanning solar air heaters, gas turbines, and microfluidic systems for advanced thermal management. The most notable features of such configurations is the presence of mixed convection, which results from the combined effects of buoyancy-induced flow caused by temperature gradients and externally imposed pressure-driven flow. These dynamics are particularly evident in open cavities where heated surfaces interact with cooler channel flow, creating intricate recirculation patterns.

The investigation of flow and thermal transport in open cavities, particularly in combination with horizontal channels, has been a focus of many studies. For instance,

Subhasree Dutta, Department of Basic Science and Humanities, University of Engineering and Management, Kolkata-700160, India; and Institute of Engineering and Management, Kolkata-700160, India, e-mail: subhasree.dutta@uem.edu.in

https://doi.org/10.1515/9783112213179-018

Burgos et al. [5] employed the lattice Boltzmann method to study mixed convection. Furthermore, Rahman et al. [20] investigated the effects of magnetic fields and Joule heating on the thermal behavior of a channel-cavity configuration. Their study revealed that magnetic fields generally suppress fluid circulation inside the cavity, thereby reducing the efficiency of thermal performance. Further, Rahman et al. [21] discussed the role of heater configuration, demonstrating that the use of localized heaters on the cavity boundaries leads to significant improvements, particularly at elevated Rayleigh numbers.

Experimental studies have played a crucial role in advancing the understanding of mixed convection within open cavities. For instance, Manca et al. [16] investigated how variations in the aspect ratio of open cavities impact heat transfer characteristics. Their analysis identified specific parameter ranges that maximize thermal performance. Likewise, Hussain et al. [13] investigated the impact of magnetic fields on mixed convection within rectangular open cavities. Their findings revealed that heat transfer performance peaks when no magnetic field is present, whereas higher Hartmann numbers lead to restricted fluid motion and diminished heat transfer rates.

Nanofluids, consisting of nanoparticles dispersed within a host liquid, possess enhanced thermal characteristics compared to traditional fluids. This enhancement arises from the superior thermal conductivity of nanoparticles, which significantly boosts the heat transfer potential of the fluid [10, 24]. Extensive investigations have been performed to analyze nanofluids particularly in enclosures with differential heating [22, 7, 3]. The two-phase modeling approach provides a comprehensive framework by incorporating particle slip effects to capture behavior of nanofluids more accurately [4].

Non-Newtonian nanofluids have garnered increasing attention due to their complex rheological properties and relevance in industrial and biomedical applications. Unlike Newtonian fluids, where viscosity is constant, non-Newtonian fluids exhibit viscosity dependent on shear rates, often described using models such as the Bingham, Herschel–Bulkley, and Casson models. Applications of Casson fluids include blood flow modeling, particle suspensions, and the design of lubricants and food products [23, 1].

Despite the extensive research on fluids, studies addressing the mixed convection of viscoplastic nanofluids in complex geometries, such as grooved or open channels, remain limited. This gap is particularly evident for configurations involving heat-generating walls, where the interplay of buoyancy- and shear-driven flows becomes more complex. Additionally, although many studies rely on homogeneous assumptions for numerical modeling, these approaches often neglect the critical effects of Brownian diffusion and thermophoresis, which are significant in nonhomogeneous nanoparticle distributions [2].

Our research incorporates a nonhomogeneous two-phase model to account for nanoparticle slip velocity and a temperature-dependent plastic viscosity model to capture the complex rheological behavior of viscoplastic nanofluids. Furthermore, the study evaluates thermal performance through entropy generation and pressure drop analysis, providing insights into optimizing heat transfer and energy efficiency in grooved channel systems.

2 Mathematical formulation

The computational domain under consideration comprises a two-dimensional horizontal channel with aspect ratio $L/H = 6$. A rectangular open-ended enclosure, filled with a temperature-dependent viscoplastic nanofluid, is connected to the channel (see Figure 19.1). The bottom surfaces, including the three cavity wells and the lower channel walls are heated with temperature T_h, where the upper is assumed to be thermally insulated and impermeable.

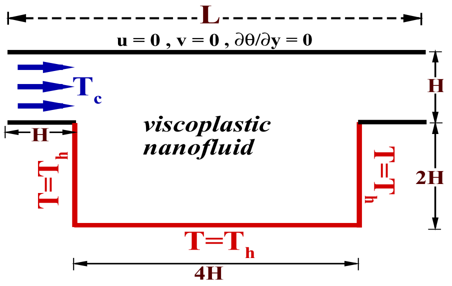

Figure 19.1: Sketch of the computational setup.

The fluid used is a mixture of ethylene glycol containing suspended alumina nanoparticles (Al_2O_3), introduced into the channel with a steady velocity U_0. A condition of zero diffusion flux is applied to all physical parameters at the outlet. The channel and the adjoining enclosure are filled with the nanofluid described by Buongiorno's two-phase model, enabling spatial variations in nanoparticle concentration. At higher concentrations of Al_2O_3 nanoparticles, ethylene glycol-based nanofluids exhibit viscoplastic characteristics. To maintain Newtonian fluid behavior, φ_b is constrained to $0 \leq \varphi_b \leq 0.06$.

$$\nabla \cdot \mathbf{u}^* = 0, \tag{19.1}$$

$$\frac{\partial(\rho_{nf}\mathbf{u}^*)}{\partial t^*} + \mathbf{u}^* \cdot \nabla(\rho_{nf}\mathbf{u}^*) = -\nabla p^* + \nabla \cdot \tau_{ij} + (\rho\beta)_{nf}(T - T_c) \cdot e_g, \tag{19.2}$$

$$\frac{\partial((\rho C_p)_{nf}T)}{\partial t^*} + \mathbf{u}^* \cdot \nabla((\rho C_p)_{nf}T) = \nabla \cdot (k_{nf}\nabla T) - C_p J_p \cdot \nabla T, \tag{19.3}$$

$$\rho_p \frac{\partial \varphi^*}{\partial t^*} + \rho_p(\mathbf{u}^* \cdot \nabla\varphi^*) = -\nabla \cdot J_p. \tag{19.4}$$

The Casson model [6] is utilized to characterize the flow behavior of viscoplastic fluids with defined yield stress. Relation between stress and strain for viscoplastic materials governed by this model is represented as

$$\tau^{*1/n} = \tau_0^{*1/n} + (\mu_p \dot{\gamma})^{1/n}, \tag{19.5}$$

which leads to the following representation:

$$\tau^* = \left[(\mu_p)^{1/n} + \left(\frac{\tau_0^*}{|\dot{\gamma}^*|} \right)^{1/n} \right]^n \dot{\gamma}^* \quad \text{for yielded region,}$$

and

$$\dot{\gamma}^* = 0 \quad \text{for unyielded region.}$$

In this model, τ_0^* represents yield stress, and setting $\tau_0^* = 0$ reduces the model to Newtonian behavior. The modified Casson–Papanastasiou model as proposed by Papanastasiou [18] is given by

$$\tau^* = \left[\sqrt{\mu_p} + \sqrt{\frac{\tau_0^*}{|\dot{\gamma}^*|}(1 - \exp(-m|\dot{\gamma}|))} \right]^2 \dot{\gamma}^*$$

with μ_p varying with temperature and represented using the relation [14, 17]

$$\mu_p(T) = \mu_p^0 \exp\{-b(T - T_c)\},$$

where μ_p^0 is the reference viscosity at a specific temperature T_c, and b is the temperature-viscosity coefficient [15]. Substituting this temperature-dependent viscosity into the generalized form of the Casson model, the shear stress expression becomes

$$\tau^* = \left[\sqrt{\mu_p^0 \exp\{-b(T - T_c)\}} + \sqrt{\frac{\tau_0^*}{|\dot{\gamma}^*|}(1 - \exp(-m|\dot{\gamma}|))} \right]^2 \dot{\gamma}^*.$$

Rewrite the equations in the nondimensional form as

$$\frac{\partial u}{\partial x} + \frac{\partial v}{\partial y} = 0, \tag{19.6}$$

$$\begin{aligned} &\frac{\partial}{\partial t}\left(\frac{\rho_{nf}}{\rho_f} u\right) + u\frac{\partial}{\partial x}\left(\frac{\rho_{nf}}{\rho_f} u\right) + v\frac{\partial}{\partial y}\left(\frac{\rho_{nf}}{\rho_f} u\right) \\ &\quad = -\left(\frac{\rho_{nf}}{\rho_f}\right)\frac{\partial p}{\partial x} + \frac{1}{Re}\left[\frac{\partial}{\partial x}\left\{\frac{\mu_{nf}}{\mu_f}\left(2\mu_f \frac{\partial u}{\partial x}\right)\right\} + \frac{\partial}{\partial y}\left\{\frac{\mu_{nf}}{\mu_f}\left(\mu_f\left(\frac{\partial u}{\partial y} + \frac{\partial v}{\partial x}\right)\right)\right\}\right], \end{aligned} \tag{19.7}$$

$$\frac{\partial}{\partial t}\left(\frac{\rho_{nf}}{\rho_f}v\right)+u\frac{\partial}{\partial x}\left(\frac{\rho_{nf}}{\rho_f}v\right)+v\frac{\partial}{\partial y}\left(\frac{\rho_{nf}}{\rho_f}v\right)$$
$$=-\left(\frac{\rho_{nf}}{\rho_f}\right)\frac{\partial p}{\partial y}+\frac{1}{Re}\left[\frac{\partial}{\partial x}\left\{\frac{\mu_{nf}}{\mu_f}\left(\mu_f\left(\frac{\partial u}{\partial y}+\frac{\partial v}{\partial x}\right)\right)\right\}+\frac{\partial}{\partial y}\left\{\frac{\mu_{nf}}{\mu_f}\left(2\mu_f\frac{\partial v}{\partial y}\right)\right\}\right]+Ri\frac{(\rho\beta)_{nf}}{\rho_f\beta_f}\theta, \tag{19.8}$$

$$\frac{\partial}{\partial t}\left(\frac{(\rho C_p)_{nf}}{(\rho C_p)_f}\theta\right)+u\frac{\partial}{\partial x}\left(\frac{(\rho C_p)_{nf}}{(\rho C_p)_f}\theta\right)+v\frac{\partial}{\partial y}\left(\frac{(\rho C_p)_{nf}}{(\rho C_p)_f}\theta\right)$$
$$=\frac{1}{Re\cdot Pr}\left[\frac{\partial}{\partial x}\left(\frac{k_{nf}}{k_f}\frac{\partial\theta}{\partial x}\right)+\frac{\partial}{\partial y}\left(\frac{k_{nf}}{k_f}\frac{\partial\theta}{\partial y}\right)\right]+\frac{1}{Re\cdot Pr\cdot Le}\left[\frac{\partial\theta}{\partial x}\frac{\partial\varphi}{\partial x}+\frac{\partial\theta}{\partial y}\frac{\partial\varphi}{\partial y}\right] \tag{19.9}$$
$$+\frac{1}{Re\cdot Pr\cdot Le\cdot N_{BT}}\left[\left(\frac{\partial\theta}{\partial x}\right)^2+\left(\frac{\partial\theta}{\partial y}\right)^2\right],$$

$$\frac{\partial\varphi}{\partial t}+u\frac{\partial\varphi}{\partial x}+v\frac{\partial\varphi}{\partial y}=\frac{1}{Re\cdot Sc}\left(\frac{\partial^2\varphi}{\partial x^2}+\frac{\partial^2\varphi}{\partial y^2}\right)+\frac{1}{Re\cdot Sc\cdot N_{BT}}\left(\frac{\partial^2\theta}{\partial x^2}+\frac{\partial^2\theta}{\partial y^2}\right). \tag{19.10}$$

Corcione's model [8], suitable for the present configuration, is employed to compute the thermal conductivity:

$$\frac{k_{nf}}{k_f}=1+4.4Re_b^{0.4}Pr^{0.66}\left(\frac{T}{T_{fr}}\right)^{10}\left(\frac{k_p}{k_f}\right)^{0.03}\varphi^{0.66}.$$

The effective viscosity and the dimensionless viscosity are presented by the correlations

$$\mu_{nf}=\frac{\mu_f}{1-34.87(\frac{d_p}{d_f})^{-0.03}\varphi^{1.03}},$$
$$\mu_f=\left[\sqrt{\exp(-P_n\theta)}+\sqrt{\frac{Ca}{|\dot\gamma|}}(1-\exp(-M|\dot\gamma|))\right]^2,$$

where $P_n=b\Delta T$ (the Pearson number) quantifies the temperature dependence of viscosity.

For the boundary condition of volume fraction:

$$\frac{\partial\varphi}{\partial n}+\frac{1}{N_{BT}}\frac{\partial\theta}{\partial n}=0.$$

At inlet:

$$\theta=0,\quad u=1,\quad v=0,\quad \frac{\partial\varphi}{\partial x}=-\frac{1}{N_{BT}}\frac{\partial\theta}{\partial x}.$$

At outlet:

$$\frac{\partial\theta}{\partial x}=0,\quad \frac{\partial u}{\partial x}=0,\quad \frac{\partial v}{\partial x}=0,\quad \frac{\partial\varphi}{\partial x}=0.$$

The governing equations are discretized using the finite volume method on a staggered grid, following a technique similar to that outlined by Dutta et al. [9]. The SIMPLE algorithm [11] is used to couple the velocity and pressure corrections, whereas for approximating the convective terms, the QUICK scheme [12] is used. Iterative calculations proceed until the convergence criteria are met, ensuring that the velocity field is divergence-free.

3 Comparative study and grid independency test

The computational domain is discretized using uniform grids of sizes 51×306, 101×606, and 151×906, where the first and second numbers denote grid points along the x- and y-directions, respectively. For $\varphi_b = 0.05$, $Re = 100$, $Ri = 1$, $Ca = 10$, and $d_p = 60$ nm, the results in Figure 19.2a indicate negligible differences in Nu for grid refinement beyond 101×606, confirming its adequacy for the current study.

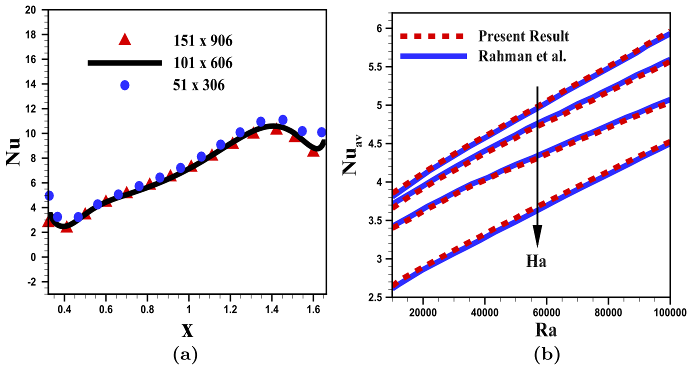

Figure 19.2: (a) The grid independence study for Nu at $Ri = 1$, $\varphi_b = 0.05$, $Ca = 10$, and $Re = 100$; (b) Comparison of Nu_{av} against the Rayleigh number for varying Hartmann numbers at $Re = 100$ with Rahman et al. [19].

To validate the numerical method and algorithm, the computed Nu_{av} at $Re = 100$ is compared with the findings of Rahman et al. [19]. Their study focused on mixed convection heat transfer in a channel featuring an open cavity heated from below and subjected to a perpendicular magnetic field (see Figure 19.2b). The close agreement between the results confirms the reliability and accuracy of the proposed numerical scheme.

4 Results and discussions

Our research examines rheological behavior of a viscoplastic nanofluid, modeled as nonhomogeneous, with properties influenced by nanoparticle concentration and diameter. Specifically, the thermal characteristics of an Al_2O_3-ethylene glycol nanofluid are analyzed, focusing on its capacity to facilitate the transfer of thermal energy from the heated wall of the cavity to the cooler fluid flowing through the channel. Key parameters considered include the Casson number Ca, Pearson number Pn, nanoparticle diameter d_p, bulk concentration φ_b, and Reynolds number Re.

4.1 Flow behavior and isotherms

The flow field characteristics in the grooved (or open) channel system vary significantly with changes in Re, Ca, and Ri, resulting in distinct yielded and unyielded regions that impact heat transfer efficiency. From Figure 19.3 it is evident that at lower Re, the flow remains primarily influenced by viscous forces, and the higher yield stress associated with increased Ca restricts fluid motion, creating substantial unyielded regions near the channel walls and grooves where shear stress does not exceed the yield threshold. These stagnant, unyielded zones, which impede fluid motion and convective heat transfer, expand with increasing Ca, leading to localized areas of minimal flow within the grooves.

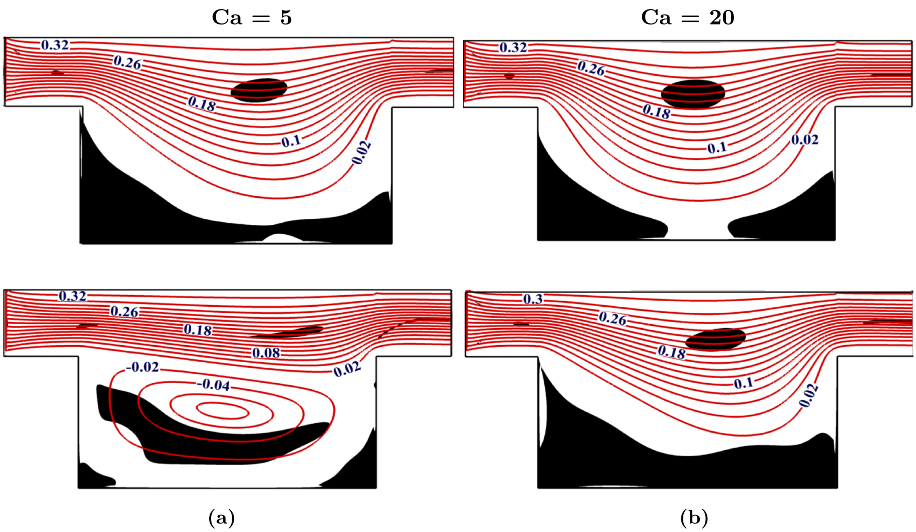

Figure 19.3: Flow fields for the Reynolds number $Re = 100$ (first row) and 500 (second row) and the Casson number (a) $Ca = 5$ and (b) $Ca = 20$, respectively, at $\varphi_b = 0.01$, $Ri = 1$, $Pn = 1$, and $d_p = 30$ nm.

As *Re* rises, inertia dominates, disrupting unyielded regions and enhancing circulation within the channel. This transition fosters more active mixing, which enables previously stagnant areas to contribute to convective heat transfer, yielding a more uniform flow distribution. Additionally, the Richardson number (*Ri*) further adjusts the flow by balancing buoyancy and inertia. At low *Ri*, inertia-driven flow smooths out transitions across the channel, producing minimal recirculation, while higher *Ri* values amplify buoyancy effects, forming thermal plumes that drive recirculation within the grooves. These plumes increase mixing and heat transport, particularly near heated channel walls. When both *Ri* and *Ca* are elevated, buoyancy and yield stress create intricate flow patterns with alternating yielded and unyielded zones across the channel and grooves. This complex interaction among inertia, buoyancy, and yield stress leads to layered flow structures, significantly affecting heat transfer and temperature distribution throughout the open channel.

Expanding on the analysis presented in Figure 19.4, the thermal field in the grooved channel shows pronounced differences in temperature distribution and heat transfer mechanisms across different values of *Ri* and *Ca*. At low Richardson number, where the flow is largely inertia-driven, the thermal field remains relatively uniform across the channel due to forced convection, which limits the development of strong thermal gradients.

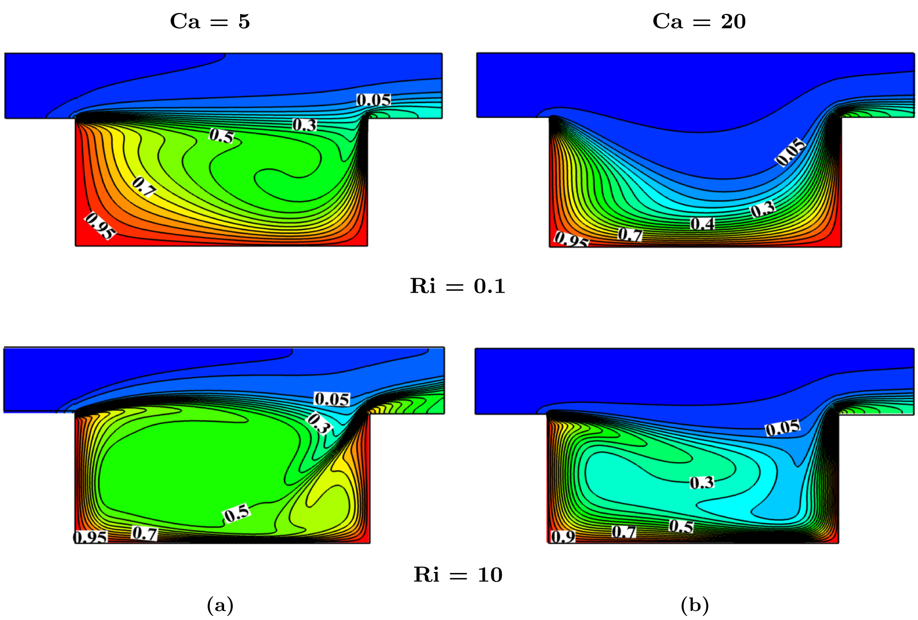

Figure 19.4: Thermal field for $Ri = 0.1$ and $Ri = 10$ and the Casson numbers (a) $Ca = 5$ and (b) $Ca = 20$, respectively, at $\varphi_b = 0.01$, $Ri = 1$, $Pn = 1$, and $d_p = 30$ nm.

As *Ri* increases, buoyancy effects become more prominent, resulting in the formation of buoyant thermal plumes that rise from the heated groove walls. These plumes create upward convective currents, generating stratified temperature regions with hotter fluid accumulating near the grooves and cooler fluid moving toward the center of the channel. This buoyancy-driven movement not only intensifies mixing near the heated walls but also creates temperature gradients that vary significantly along the channel height, producing a more complex thermal field with alternating zones of hot and cool fluid.

The Casson number *Ca* further influences the thermal field by affecting the fluid yield behavior. At higher *Ca* values, where yield stress is significant, unyielded regions form near the groove walls, restricting flow and limiting heat transfer in these zones. This leads to thermal insulation effects in areas where fluid motion is suppressed, with the temperature remaining high near the heated surfaces. In these regions, heat transfer is increasingly dependent on conduction rather than convection, as the fluid' s movement is restricted by yield stress. This yields sharper temperature contrasts between the yielded and unyielded regions, with hot zones trapped near the grooves due to limited mixing.

The combined effect of high *Ri* and high *Ca* creates a distinct thermal stratification pattern with well-defined hot layers near the groove walls and cooler regions in the main flow channel. These complex thermal structures reflect the interplay between buoyancy forces, yield stress, and inertial forces, making the thermal field highly sensitive to changes in both *Ri* and *Ca*. This sensitivity impacts the overall heat transfer performance across the channel, highlighting the need for careful tuning of these parameters in applications that rely on effective thermal management within grooved or open channel systems.

4.2 Heat transfer

The thermal performance in the grooved channel, as reflected by the Nusselt number *Nu* in Figure 19.5a–c, reveals complex interactions between φ_b, d_p, *Re*, *Ca*, and *Pn*. The results demonstrate that heat transfer is strongly influenced by the nonhomogeneous model, especially with varying nanoparticle properties and flow parameters.

In Figure 19.5a, it is evident that as φ_b increases, the average Nusselt number Nu_{av} also increases, indicating an enhancement in heat transfer due to increased thermal conductivity provided by higher nanoparticle concentration. However, this effect is dependent on d_p: smaller nanoparticle diameters, such as $d_p = 30$ nm, yield greater Nu_{av} values compared to larger diameters. This enhancement is more prominent in the nonhomogeneous model, suggesting that the inclusion of Brownian motion and thermophoresis effects in nanoparticle dispersion significantly contributes to improved heat transfer performance.

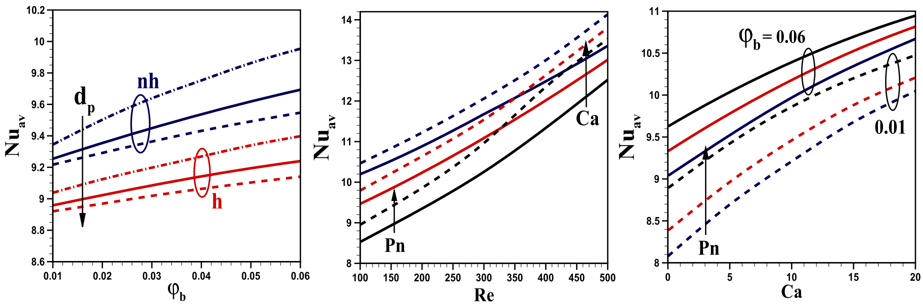

Figure 19.5: Variation of Nu_{av} with (a) φ_b for different values of $d_p = 30$ (dash-dotted lines), $d_p = 90$ (solid lines), and $d_p = 150$ (dashed lines) at $Ca = 10$, $Pn = 1$, $Ri = 1$, and $Re = 100$ for the two-phase (blue lines) and single-phase (red lines) models; (b) Re for the Casson numbers $Ca = 1, 10, 20$ at $Pn = 1$ (solid lines) and 4 (dashed lines) at $d_p = 30$ nm, $Ri = 1$, and $\varphi_b = 0.01$; (c) Ca for $Pn = 0, 1, 10$ and $\varphi_b = 0.01, 0.06$ at $Re = 100$ and $Ri = 1$.

With respect to Re, the results indicate a substantial increase in Nu_{av} as Re increases, particularly for higher Ca values (Figure 19.5b). At lower Ca, the fluid exhibits more unrestricted flow, allowing for effective convective heat transfer that scales with Re. However, as Re increases, these unyielded zones are minimized, enhancing circulation and, consequently, the heat transfer rate. The effect of Pn is also notable: for larger Pn, which reflects the temperature-dependent viscosity, the Nu_{av} values are slightly reduced, especially at higher Ca values, due to the increased flow resistance from temperature-induced viscosity variations.

The results in Figure 19.5c show that for increasing Ca with constant φ_b and d_p, there is a decrease in Nu_{av}, indicating the influence of yield stress in reducing convective transport near the grooved walls. This reduction is more pronounced at higher Ca and lower Re, where the formation of unyielded regions reduces the effective heat transfer surface area. The combined impact of Pn and Ca on Nu_{av} underscores the role of yield stress and temperature-dependent viscosity in moderating flow dynamics, especially under conditions where buoyancy effects contribute less to overall heat transfer.

In summary, the heat transfer characteristics in the grooved channel are maximized by optimizing nanoparticle concentration, Reynolds number, and nanoparticle diameter. High Re and low Ca values are particularly effective for enhancing Nu_{av}, as they promote convective mixing. The results confirm the significant impact of the nonhomogeneous model in capturing realistic heat transfer behavior, with Brownian diffusion and thermophoresis effects critical to maximizing thermal performance in this complex flow system.

5 Conclusions

This research provides a comprehensive analysis of the flow dynamics, thermal behavior, and heat transfer properties of viscoplastic nanofluids within a grooved channel, using a nonhomogeneous two-phase model to incorporate nanoparticle slip effects. The results reveal that the flow field is significantly influenced by the Reynolds number Re, Casson number Ca, and Richardson number Ri, with higher Ca creating extensive unyielded zones near the groove walls, whereas higher Re promotes mixing and reduces flow stagnation. The thermal field demonstrates pronounced stratification at higher Ri, driven by buoyancy-induced thermal plumes, which enhance heat transfer near heated walls but lead to localized insulation effects in unyielded regions at higher Ca.

The heat transfer analysis through the average Nusselt number Nu_{av} shows that higher nanoparticle volume fractions φ_b and smaller nanoparticle diameters d_p significantly enhance thermal performance with the nonhomogeneous model. Heat transfer is maximized under high Re and low Ca, where convective mixing is strongest, and unyielded zones are minimized. These findings underline the critical roles of nanoparticle properties and flow parameters in determining thermal efficiency and offer practical guidance for optimizing the design of grooved channels in thermal management applications. This study also highlights the importance of using nonhomogeneous models to capture the intricate interactions in complex flow systems, providing a robust framework for future research and industrial applications.

Bibliography

[1] Aghighi, M. S., Metivier, C., Masoumi, H.: Natural convection of Casson fluid in a square enclosure. *Multidiscip. Model. Mater. Struct.* 16(5), 1245–1259 (2020)

[2] Akbari, M., et al.: Influence of slip conditions and nonhomogeneous modeling on the heat transfer performance of nanofluid flow. *Appl. Therm. Eng.* 170, 115036 (2020)

[3] Ben-Cheikh, N., Chamkha, A. J., Ben-Beya, B., Lili, T.: Natural convection of water-based nanofluids in a square enclosure with non-uniform heating of the bottom wall. *J. Mod. Phys.* 4(2), 147 (2013)

[4] Buongiorno, J.: Convective transport in nanofluids. *J. Heat Transf.* 128(3), 240–250 (2006)

[5] Burgos, J., Cuesta, I., Salueña, C.: Numerical study of laminar mixed convection in a square open cavity. *Int. J. Heat Mass Transf.* 99, 599–612 (2016)

[6] Casson, N.: A flow equation for pigment-oil suspensions of the printing ink type. In: Mill, I. K. C. C. (ed.) *Rheology of Disperse Systems*, pp. 84–104. Pergamon Press, Elmsford, NY (1959)

[7] Cho, C. C.: Heat transfer and entropy generation of natural convection in nanofluid-filled square cavity with partially-heated wavy surface. *Int. J. Heat Mass Transf.* 77, 818–827 (2014)

[8] Corcione, M.: Empirical correlating equations for predicting the effective thermal conductivity and dynamic viscosity of nanofluids. *Energy Convers. Manag.* 52(1), 789–793 (2011)

[9] Dutta, S., Bhattacharyya, S., Pop, I.: Nonhomogeneous model for conjugate mixed convection of nanofluid and entropy generation in an enclosure in presence of inclined magnetic field with Joule heating. *Int. J. Numer. Methods Heat Fluid Flow* 31(1), 418–441 (2021)

[10] Esfe, M. H., Saedodin, S., Malekshah, E. H., Babaie, A., Rostamian, H.: Mixed convection inside lid-driven cavities filled with nanofluids. *J. Therm. Anal. Calorim.* 135(1), 813–859 (2019)

[11] Fletcher, C. A.: *Computational Techniques for Fluid Dynamics 2: Specific Techniques for Different Flow Categories*. Springer (2012)

[12] Hayase, T., Humphrey, J. A. C., Greif, R.: A consistently formulated QUICK scheme for fast and stable convergence using finite-volume iterative calculation procedures. *J. Comput. Phys.* 98(1), 108–118 (1992)

[13] Hussain, S., Ahmed, S. E., Akbar, T.: Entropy generation analysis in MHD mixed convection of hybrid nanofluid in an open cavity with a horizontal channel containing an adiabatic obstacle. *Int. J. Heat Mass Transf.* 114, 1054–1066 (2017)

[14] Labsi, N., Benkahla, Y. K., Boutra, A.: Viscous dissipation effect on the flow of a thermodependent Herschel–Bulkley fluid. *Therm. Sci.* 19(5), 1553–1564 (2015)

[15] Labsi, N., Benkahla, Y. K., Boutra, A., Ammouri, A.: Heat and flow properties of a temperature dependent viscoplastic fluid including viscous dissipation. *J. Food Process Eng.* 36(4), 450–461 (2013)

[16] Manca, O., Nardini, S., Khanafer, K., Vafai, K.: Effect of heated wall position on mixed convection in a channel with an open cavity. *Numer. Heat Transf., Part A, Appl.* 43(3), 259–282 (2003)

[17] Métivier, C., Nouar, C.: Linear stability of the Rayleigh–Bénard Poiseuille flow for thermodependent viscoplastic fluids. *J. Non-Newton. Fluid Mech.* 163(1–3), 1–8 (2009)

[18] Papanastasiou, T. C.: Flows of materials with yield. *J. Rheol.* 31(5), 385–404 (1987)

[19] Rahman, M. M., Parvin, S., Saidur, R., Rahim, N. A.: Magnetohydrodynamic mixed convection in a horizontal channel with an open cavity. *Int. Commun. Heat Mass Transf.* 38(2), 184–193 (2011)

[20] Rahman, M. M., Saidur, R., Rahim, N. A.: Conjugated effect of joule heating and magneto-hydrodynamic on double-diffusive mixed convection in a horizontal channel with an open cavity. *Int. J. Heat Mass Transf.* 54(15–16), 3201–3213 (2011)

[21] Rahman, M. M., Öztop, H. F., Saidur, R., Mekhilef, S., Al-Salem, K.: Finite element solution of MHD mixed convection in a channel with a fully or partially heated cavity. *Comput. Fluids* 79, 53–64 (2013)

[22] Rao, S. S., Srivastava, A.: Interferometric study of natural convection in a differentially-heated cavity with Al_2O_3–water based dilute nanofluids. *Int. J. Heat Mass Transf.* 92, 1128–1142 (2016)

[23] Sankar, D. S., Lee, U., Ismail, A. I. M.: Mathematical analysis for MHD flow of blood in constricted arteries. *Int. J. Nonlinear Sci. Numer. Simul.* 14(3–4), 195–204 (2013)

[24] Yang, L., Du, K.: A comprehensive review on the natural, forced, and mixed convection of non-Newtonian fluids (nanofluids) inside different cavities. *J. Therm. Anal. Calorim.* 140, 2033–2054 (2020)